

A handheld polarized hyperspectral imaging probe for tissue differentiation using spectral and polarization characteristics

Ling Ma ^{a,b}, Izabella Chaverra ^{a,b}, Chinmay Patwardhan ^{a,b},
Rokunuzjahan Rudro ^{a,b}, Amie Ha ^{a,b}, Suhani Swain ^{a,b}, Baowei Fei ^{a,b,c,*}

^a Center for Imaging and Surgical Innovation, University of Texas at Dallas, Richardson, TX

^b Department of Bioengineering, University of Texas at Dallas, Richardson, TX

^c Department of Radiology, University of Texas Southwestern Medical Center, Dallas, TX

*Corresponding author: bfei@utdallas.edu, Website: <https://fei-lab.org>

ABSTRACT

Polarized hyperspectral imaging (PHSI) integrates spectral and polarization contrast to enable comprehensive tissue characterization. In this study, we validate a refined handheld PHSI probe that is more compact, lightweight, and capable of rapid image acquisition. The system was evaluated on freshly excised tissues from five male mice, focusing on four organ types—brain, tongue, thyroid, and testicle—chosen for their similar macroscopic appearance but distinct biochemical and microstructural properties. Spectral classification was performed using a one-dimensional convolutional neural network (1D-CNN) trained on total reflectance (Stokes S_0) spectra. In parallel, polarization-resolved parameters—degree of linear polarization (DoLP) and degree of circular polarization (DoCP)—were derived to visualize structural and scattering differences among tissues. Despite the visual similarity among tissues, the model achieved high classification accuracy with an average overall accuracy of 95.3% across leave-one-out cross-validation folds. DoLP effectively differentiated glandular from adipose tissue, and highlighted muscle fiber orientation differences within tongue regions. DoCP distinguished blood-rich regions from surrounding glandular or fatty tissues, revealing higher DoCP in vascular areas and lower values in fat. These results confirm that spectral and polarization features offer complementary tissue contrast. This work demonstrates the potential of handheld PHSI for real-time tissue assessment and lays the foundation for future integration of spectral and polarization data in machine learning for clinical decision support.

Keywords: Polarized hyperspectral imaging (PHSI), handheld device, tissue characterization, spectral classification, degree of linear polarization (DoLP), degree of circular polarization (DoCP)

1. INTRODUCTION

Polarized hyperspectral imaging (PHSI) is an optical imaging technique that captures images across a broad range of wavelengths while utilizing polarized light to detect subtle variations in tissue structure and composition.^{1,2} By combining hyperspectral imaging (HSI) and polarized light imaging (PLI), PHSI provides complementary information on tissue properties such as scattering behavior and molecular content, which are largely undetectable with conventional imaging modalities.³ PHSI has shown promise in medical diagnostics and tissue microstructure analysis,^{4,5} yet its broader adoption has been limited by the size, cost, and complexity of existing systems. The development of a handheld platform could overcome these barriers and enable real-time, label-free imaging in clinical settings, where portability and ease of use are essential for intraoperative or point-of-care applications.

In this study, we refined our previously developed handheld PHSI probe and validated its capability for tissue characterization based on both spectral and polarization signatures. Freshly excised mouse organs with distinct tissue types were imaged. Spectral reflectance features, along with polarization parameters such as degree of linear polarization (DoLP) and degree of circular polarization (DoCP), were extracted for tissue differentiation. The results demonstrate the feasibility of compact PHSI for probing intrinsic tissue contrast. This work is an important step for future applications of real-time, handheld PHSI systems in surgical guidance and clinical diagnostics.

2. METHODS

Handheld polarized hyperspectral imaging probe

We developed a handheld PHSI probe capable of full-Stokes imaging. The optical system consists of two liquid crystal variable retarders (LCVRs), a linear polarizer, a focusing lens, and a snapshot mosaic hyperspectral camera. The camera operates in the visible light range from 460 to 600 nm and captures 16 spectral bands with an image resolution of 510 pixels \times 210 pixels.⁶

To minimize ambient light interference, the optical tube was 3D printed using matte black PLA filament and lined with a light-absorbing material. A compact, ring-shaped illuminator with an integrated linear polarizer was attached to the front of the probe. The complete probe assembly is compact, measuring less than 180 mm in length, and is lightweight for ease of handheld operation. It has a field of view of 7 mm \times 11 mm, as well as a decent resolution of 7.13 lp/mm. Both LCVRs were calibrated at 530 nm. Their fast axes, along with the transmissive axis of the linear polarizer, were carefully aligned and fixed using a custom-designed retaining ring. The acquisition of four polarization-resolved images required for full-Stokes reconstruction is completed in under 0.5 seconds. The entire imaging process—including acquisition, white and dark reference calibration, hypercube demosaicking, and data saving—is fully automated using custom software and takes less than 1 second per measurement.

Prior to tissue imaging, the wavelength-dependent error of the assembled probe was evaluated using a spectrometer. Then, its spectral and polarization measurement capabilities were validated using standard color tiles and lipid emulsion phantoms. The results demonstrated high spectral fidelity and reliable detection of varying levels of depolarization.⁷

PHSI data acquisition

Five male mice were euthanized, and various organs were collected postmortem immediately. For this study, we focused on four organs—brain, tongue, thyroid, and testicle—selected for their similar visible appearance yet differing biochemical and microstructural properties. Tongue and both testicles were successfully collected from all five mice. Brain data was unavailable for mouse #4, and thyroid tissue was only available from three mice. As a result, thyroid data were included in the polarization-resolved tissue characterization but excluded from the machine learning-based spectral classification analysis.

During image acquisition, tissue samples were placed on a matte black plastic board to minimize background reflectance, given the thinness and partial translucency of the samples. The handheld PHSI probe was positioned directly over each tissue, and each acquisition (including subsequent automatic processing) took approximately 0.75 seconds. Prior to tissue imaging, white and dark reference images were acquired using a white diffuse reflectance standard tile and with the probe shuttered, respectively, both taken with the LCVRs set to zero retardance.

Following the acquisition, glare detection based on total intensity and anomalously high Stokes S2 values were carried out to mask specular reflections. Tissue regions were manually segmented, and average spectra were extracted from non-overlapping 10 \times 10 pixel patches within each tissue mask. These data formed the basis for both spectral classification and polarization-based tissue characterization.

Tissue characterization using PHSI data

To investigate tissue contrast mechanisms using PHSI, we analyzed both spectral and polarization-resolved information. Spectral classification focused on the optical properties related to chromophores and biochemical composition, using the Stokes parameter S0, which represents total reflectance independent of polarization. In parallel, we derived DoLP and DoCP from the full Stokes parameters to assess tissue characteristics influenced by scattering and microstructural organization. This dual approach enables complementary insights into both biochemical and structural features of tissues.

Spectral-based tissue differentiation

A one-dimensional convolutional neural network (1D CNN) consisting of 3 convolutional layers, 2 max pooling layers, and 1 fully connected layer was implemented to classify tissue types based on their S0 spectra. The model was trained in a supervised learning fashion for 10 epochs using the Adam optimizer with a mini-batch size of 128. Leave-one-out cross-validation (LOOCV)⁸ was employed across the dataset, excluding mouse #4 due to missing brain tissue data. Training was performed on an NVIDIA RTX A4000 GPU. To evaluate the multi-class tissue differentiation performance, we used overall accuracy and class-wise sensitivity as metrics:

$$\text{Overall accuracy} = \frac{\text{All correctly classified spectra}}{\text{All spectra}}$$

$$\text{Sensitivity} = \frac{\text{True positive}}{\text{True positive} + \text{False negative}}$$

Polarization-based tissue characterization

To evaluate polarization-sensitive tissue properties, we computed the full Stokes parameters and derived DoLP and DoCP. Processed hyperspectral images acquired under four polarization states, namely the horizontal polarized (IH), vertical polarized (IV), 45-degree polarized (I45), and right circular polarized (IRC), were summed across all 16 spectral bands to produce grayscale intensity images. From these, heatmaps of polarization-based parameters, i.e., DoLP and DoCP, were generated using the following equations to visualize and compare the polarization characteristics of different tissue types, highlighting variations in scattering and microstructural organization.

$$S = \begin{bmatrix} S_0 \\ S_1 \\ S_2 \\ S_3 \end{bmatrix} = \begin{bmatrix} I_H + I_V \\ I_H - I_V \\ I_{45} * 2 - S_0 \\ I_{RC} * 2 - S_0 \end{bmatrix}$$

$$DoLP = \sqrt{S_1^2 + S_2^2} / \sqrt{S_0^2}$$

$$DoCP = \sqrt{S_3^2} / \sqrt{S_0^2}$$

3. RESULTS

The handheld PHSI probe was evaluated on the freshly excised mouse tissues to assess its capability for tissue differentiation and characterization. Four organs with similar appearances and colors but different tissue types were selected, i.e., the brain, tongue, thyroid, and testicle, as shown in Figure 1. It can be seen in Figure 1(a) that the probe reveals differences at various light polarization states, especially the 45-degree polarized light image I45, as tissue rapidly depolarizes incident 45-degree linear polarization through multiple scattering and birefringence. Figure 1(b) shows RGB images synthesized from the Stokes parameter S_0 for four organs from the same mouse, all of which appear white. Nevertheless, the DOP heatmap revealed distinct tissue textures across organs. In particular, the tongue exhibited the highest DOP values, consistent with its high content of skeletal muscle. The thyroid (an endocrine gland) showed the second-highest DOP values. In contrast, the testicle (with mixed endocrine and exocrine functions) and the brain (predominantly nervous tissue) exhibited relatively lower DOP values, while the adipose tissue adjacent to the testicle displayed the lowest DOP.

Next, we performed spectral classification using Stokes parameter S_0 (total reflectance) data, while polarization-based parameters, particularly DoLP and DoCP, were predominantly used to visualize various microstructural and scattering differences among tissues. Results demonstrated that both spectral and polarization features provide complementary contrast for identifying tissue types with similar macroscopic appearance.

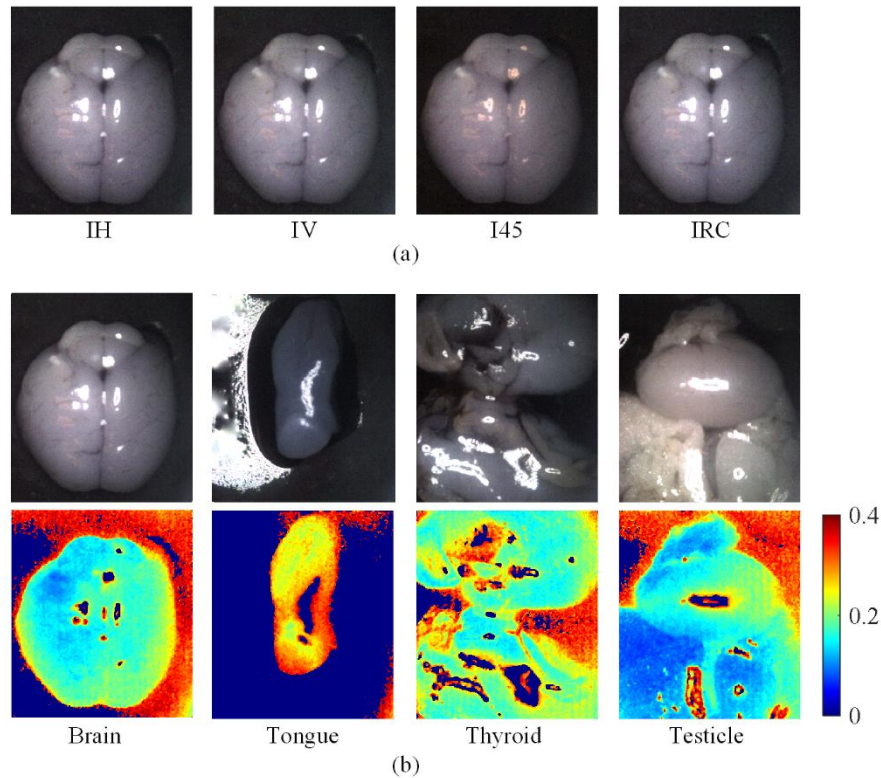


Figure 1. Illustration of tissue appearance of different light polarization states and tissue types. (a) Synthetic RGBs of the horizontal, vertical, 45-degree, and right circular polarized light images of a mouse brain under the illumination of 45-degree polarized light. (b) Synthetic RGB images of Stokes parameter S_0 and average DOP across 16 bands of four different organs from the same mouse.

Spectral classification was performed using a 1D-CNN trained on Stokes S_0 spectra to distinguish between brain, tongue, and testicle tissues. Despite the visually similar appearance of these tissues under white light, the model achieved high classification accuracy by leveraging subtle spectral differences related to biochemical composition. Across the four folds in LOOCV, the model achieved an average overall accuracy of 95.3%, with class-wise sensitivities of 97.3% for brain, 93.9% for tongue, and 92.6% for testicle tissue. These results demonstrate that the information encoded in the reflectance spectra enables reliable tissue differentiation, even in cases where tissues are not easily distinguishable by color or intensity alone. The high sensitivity across all tissue types confirms the robustness of the spectral features captured by the handheld PHSI probe.

Table 1. Spectral classification performance of mouse brain, tongue, and testicle.

Fold #	Overall accuracy	Class-wise sensitivity		
		Brain	Tongue	Testicle
1	0.943	0.904	0.921	0.994
2	0.987	0.997	0.994	0.969
3	0.950	0.992	0.879	0.926
4	0.933	0.999	0.962	0.816
Mean	0.953	0.973	0.939	0.926

Differentiation between glandular and adipose tissues was effectively achieved using polarization-based metrics, particularly the DoLP metric. In the case of testicular tissue, which contains dense glandular structures, DoLP values were consistently higher than those observed in adjacent adipose tissue, as shown in Figure 2(a-b), highlighting its potential for distinguishing tissue types with similar spectral signatures (colors) but differing microstructural organization. Similar observation was found in the mouse thyroid sample, as shown in Figure 2(c-d). Additionally, polarization imaging of the

mouse tongue revealed region-specific variations in muscle fiber orientation. The root of the tongue exhibited distinct polarization characteristics compared to the apical and middle regions, with notably higher S2 and DoLP values. This can be attributed to the orientation of muscle fibers at an angle closer to 45° relative to the incident linearly polarized light, as well as a higher concentration of glandular tissue in the root region, consistent with anatomical observations.⁹ These findings demonstrate the sensitivity of polarization parameters to both fiber alignment and glandular content within heterogeneous tissues.

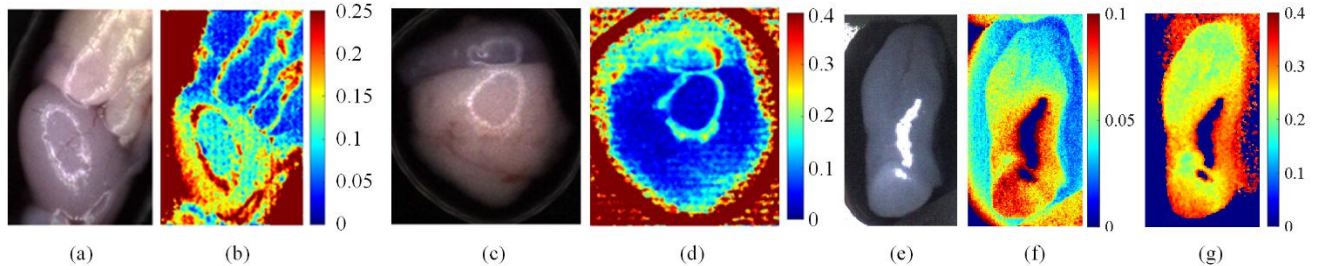


Figure 2. Differentiation of glandular tissue, adipose tissue, and muscle using the DoLP parameter. (a,b) Synthetic RGB image from HSI data and DoLP heatmap of mouse testicle and connected fat. (c,d) Synthetic RGB image and DoLP heatmap of thyroid with connective/fat tissue. (e-g) Synthetic RGB image, heatmap of S2, and DoLP heatmap of mouse tongue. Root tongue exhibiting different S2 and DoLP values due to different muscle orientation, thinner epithelium, and more glands.

The DoCP was found to be a useful parameter for distinguishing blood-rich regions from surrounding glandular and adipose tissues. As shown in Figure 3, synthetic RGB images of mouse thyroid tissues from two different animals (Figure 3a and 3c) visually highlight areas containing blood and glandular structures. The corresponding DoCP heatmaps (Figure 3b and 3d) clearly demonstrate that regions containing blood exhibit significantly higher DoCP values compared to adjacent glandular tissue. This increase in DoCP is likely due to the scattering behavior and microstructural uniformity of blood, which preserves circular polarization more effectively. In contrast, areas containing fat, such as the bottom right corner of Figure 2a, show markedly lower DoCP, reflecting the strong depolarizing nature of adipose tissue. These results suggest that DoCP can serve as an optical signature for identifying vascularized regions in complex soft tissue environments.

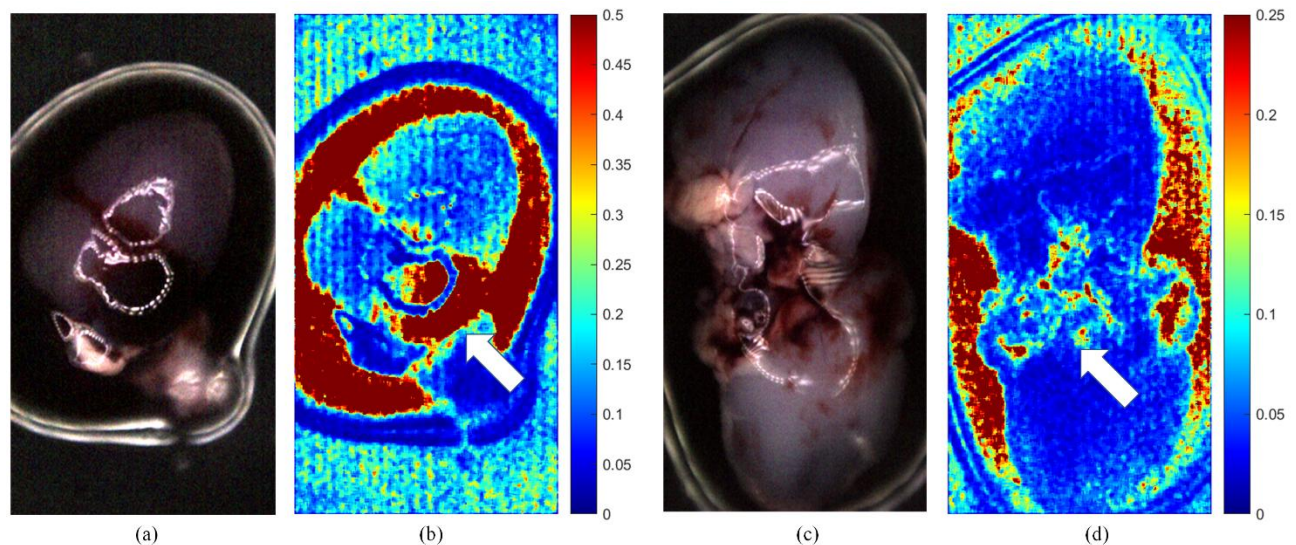


Figure 3. Differentiation of blood and glandular tissue using the DoCP parameter. (a, c) Synthetic RGB images of thyroid tissues from two different mice, both containing visible blood regions. (b, d) Corresponding DoCP heatmaps reveal significantly higher DoCP values in blood-rich areas compared to surrounding glandular tissue. White arrows indicate regions of elevated DoCP corresponding to blood, highlighting the contrast with lower DoCP values in glandular and adipose tissue.

4. DISCUSSION & CONCLUSION

This work presents the validation of a refined handheld PHSI probe designed for improved portability, speed, and usability in tissue characterization. We demonstrate its application on freshly excised mouse tissues, leveraging both spectral reflectance (Stokes S_0) and polarization-resolved metrics (DoLP and DoCP) to differentiate and characterize various tissue types. A 1D CNN was trained on S_0 spectra for tissue classification, while polarization heatmaps provided insights into microstructural differences. This study highlights the complementary contrast mechanisms provided by spectral and polarization domains and lays the groundwork for future integration of both features in machine learning models for diagnostic use on human tissues.

In this study, we enhanced our previously developed handheld polarized hyperspectral imaging probe, making it lightweight, compact, and capable of faster acquisition for tissue characterization and diagnostic applications. Multiple tissue types were imaged, and both spectral and polarization-resolved analyses were performed, demonstrating the complementary value of reflectance-based and polarization-sensitive optical properties in tissue differentiation and characterization. Future work will focus on validating the probe on *ex vivo* and *in vivo* human tissues, particularly those from head and neck cancers. In addition, we plan to explore the integration of spectral and polarization features—such as incorporating DoLP and DoCP spectra into machine learning models—to fully leverage the probe's capabilities for improved tissue characterization and disease detection.

ACKNOWLEDGMENTS

Research reported in this publication was supported in part by the National Cancer Institute of the National Institutes of Health under Award Number R01CA288379 and by the Cancer Prevention and Research Institute of Texas (CPRIT) under Award Number RP240289 and RP240542. The content is solely the responsibility of the authors and does not necessarily represent the official views of the National Institutes of Health.

REFERENCES

1. L. Ma et al., "Automated polarized hyperspectral imaging (PHSI) for ex-vivo and in-vivo tissue assessment," *Proc. SPIE* **12391** (2023).
2. X. Zhou et al., "Polarized hyperspectral microscopic imaging system for enhancing the visualization of collagen fibers and head and neck squamous cell carcinoma," *Journal of Biomedical Optics* **29**(1), 016005 (2024).
3. L. Ma et al., "Automated polarized hyperspectral imaging (PHSI) for ex-vivo and in-vivo tissue assessment," *Proc. SPIE* **12391**, 123910F (2023).
4. F. Vasefi et al., "Polarization-sensitive hyperspectral imaging in vivo: a multimode dermoscope for skin analysis," *Scientific reports* **4**(1), 1-10 (2014).
5. P. Ghassemi et al., "A polarized multispectral imaging system for quantitative assessment of hypertrophic scars," *Biomedical Optics Express* **5**(10), 3337-3354 (2014).
6. J. Sherey et al., "Validation of a handheld polarized hyperspectral imaging probe on intralipid phantom and mouse tissue," *Proc. SPIE* **13322**, 1332204 (2025).
7. L. Ma et al., "Validation of a polarized hyperspectral imaging (PHSI) probe using phantoms and biological tissues," *Proc. SPIE* **13854** (2026).
8. S. Raschka, "Model Evaluation, Model Selection, and Algorithm Selection in Machine Learning," arXiv:1811.12808 (2018).
9. H. Aoyagi, S.-i. Iwasaki, and T. Asami, "Three-Dimensional Architecture of the Mouse Tongue Muscles Using Micro-CT with a Focus on the Transverse, Vertical, and Genioglossus Muscles," *Surgical Science* **6**(8), 358-368 (2015).